PAPER

Check for updates

Novel Janus GaInX₃ (X = S, Se, Te) single-layers: first-principles prediction on structural, electronic, and transport properties

Tuan V. Vu, [ab] Nguyen N. Hieu, [*cd] A. A. Lavrentyev,[e] O. Y. Khyzhun, [f]
Chu V. Lanh,[g] A. I. Kartamyshev,[ab] Huynh V. Phuc [h] and Nguyen V. Hieu[*i]

In this paper, the structural, electronic, and transport properties of Janus GaInX₃ (X = S, Se, Te) single-layers are investigated by a first-principles calculations. All three structures of GaInX₃ are examined to be stable based on the analysis of their phonon dispersions, cohesive energy, and Born's criteria for mechanical stability. At the ground state, The Janus GaInX₃ is a semiconductor in which its bandgap decreases as the chalcogen element X moves from S to Te. Due to the vertical asymmetric structure, a difference in the vacuum level between the two surfaces of GaInX₃ is found, leading to work functions on the two sides being different. The Janus GaInX₃ exhibit high directional isotropic transport characteristics. Particularly, GaInX₃ single-layers have high electron mobility, which could make them potential materials for applications in electronic nanodevices.

1   Introduction

Two-dimensional (2D) layered materials are becoming increasingly attractive to the research community due to their extraordinary physical properties.[1–4] The diversity in the atomic structure of 2D layered materials, such as they can possess planar, buckled, the vertical symmetrical or asymmetrical structures, has created an interesting picture in the study of these systems. The successful synthesis of the vertical asymmetric Janus MoSSe[5] is an important step in expanding the family of 2D layered materials. Recent studies have shown that Janus structures have many novel physical features that do not exist in original symmetric structures.

Along with monochalcogenides and dichalcogenides, trichalcogenides have also received a lot of attention recently. In₂Se₃ nanosheets have also been successfully synthesized

ᵃDivision of Computational Physics, Institute for Computational Science, Ton Duc Thang University, Ho Chi Minh City, Vietnam. E-mail: vuvantuan@tdtu.edu.vn

ᵇFaculty of Electrical & Electronics Engineering, Ton Duc Thang University, Ho Chi Minh City, Vietnam

ᶜInstitute of Research and Development, Duy Tan University, Da Nang, Vietnam. E-mail: hieunn@duytan.edu.vn

ᵈFaculty of Natural Sciences, Duy Tan University, Da Nang, Vietnam

ᵉDepartment of Electrical Engineering and Electronics, Don State Technical University, 1 Gagarin Square, 344010 Rostov-on-Don, Russian Federation

ᶠFrantsevych Institute for Problems of Materials Science, National Academy of Sciences of Ukraine, 3 Krzhyzhanivsky Street, 03142 Kyiv, Ukraine

ᵍDepartment of Physics, Vinh University, 182 Le Duan, Vinh City, Vietnam

ʰDivision of Theoretical Physics, Dong Thap University, Dong Thap, Vietnam

ⁱPhysics Department, The University of Danang – University of Science and Education, Da Nang, Vietnam. E-mail: nvhieu@ued.udn.vn

experimentally.[6] The group-III trichalcogenides are the 2D quintuple-layer atomic materials and their crystal structure belongs to R3m space group. Due to vertical asymmetric structure, the group-III trichalcogenide single-layers possess novel physical properties that can not exist in the monochalcogenides or dichalcogenides. The group-III trichalcogenide single-layers are predicted to be stability.[7] Zhao and co-workers have revealed that the group-III trichalcogenides In₂X₃ (X = S, Se, Te) are indirect semiconductors and they are can be served as photocatalysts in the photolytic field.[8] The other group III trichalcogenide single-layers such as Al₂X₃ or Ga₂X₃ are also reported to have promising applications in water splitting and their solar-to-hydrogen efficiency is predicted to be high.[7] An intrinsic 2D out-of-plane ferroelectricity has been experimentally observed in atomically thin crystal In₂Se₃ due to the locking between in-plane lattice asymmetry and out-of-plane dipoles.[9] Based on the density functional theory, Lu and Huang have predicted that Ga₂X₃ and In₂X₃ single-layers possess excellent out-of-plane and in-plane second harmonic generation and piezoelectricity properties.[10] Recently, quintuple-layer atomic structure Ga₂O₃ has been reported to be high carrier mobility and low lattice thermal conductivity, which is suitable for applications in thermoelectric devices.[11] The vertical asymmetric structure leads to the appearance of an intrinsic electric field and dipole in the trichalcogenide and trioxide single-layers. Consequently, the adsorption energy, as well as the ability to perform water splitting applications at different surfaces of single-layers, can be different.[7,12] In parallel with the study of single-layers, van der Waals heterostructures based on the group-III trichalcogenides have also been of great interest. Ding and co-workers have previously considered the

electronic and ferroelectric characteristics of In_2Se_3/graphene and In_2Se_3/WSe_2 heterostructures. It was found that the Schottky barrier in van der Waals bilayer heterostructures based on In_2Se_3 can be modulated by switching the orientation of electric dipole in In_2Se_3 layer and they are suitable for a wide range of applications in nanoelectronics.[13]

Recently, the Janus structures of the group-III trichalcogenide single-layers have begun to be studied.[14,15] The Janus In_2X_2Y (X/Y = S, Se, Te) single-layers were confirmed to be strong solar absorption and superior out-of-plane and in-plane piezoelectric response.[14] Particularly, the electron mobility and solar-to-hydrogen efficiency of the Janus In_2X_2Y can be higher than that in In_2X_3 single-layers.[7,14] Excited by the successful synthesis of the group-III trichalcogenide nanosheets and the great recent achievements in theoretical studies on Janus group-III trichalcogenide single-layers, we here investigate the structural, electronic, and transport properties of novel Janus $GaInX_3$ (X = S, Se, Te) single-layer using the density functional theory (DFT). The obtained results not only give deep insight into the electronic and transport properties of the novel Janus $GaInX_3$ single-layers, but also provide an impetus for further both experimental and theoretical studies of this exciting family of materials.

2 Computational method

The calculations of structural optimizations and electronic structures in this work were based on the DFT approach as performed in the Quantum Espresso package.[16] The interactions between electron and ion core were treated by the projector-augmented wave pseudo-potential method.[17] The generalized gradient approximations with Perdew–Burke–Ernzerhof (PBE) functional[18] was adopted to consider the exchange-correlation function. To correct the electronic bands of the semiconductors, the Heyd–Scuseria–Ernzerhof functional (HSE06)[19] was performed in the present work. We used the DFT-D2 method with van der Waals (vdW) correction[20] to investigate the vdW interactions. A plane-wave cut-off of 50 Ry and (15 × 15 × 1) k-grid mesh in the Brillouin zone were selected for the Janus single-layers in our calculation. The atomic structures are fully relaxed until the residual forces were less than 10^{-2} eV Å^{-1}. A vacuum space of 30 Å was introduced to eliminate interactions between periodic images of slabs in the vertical direction. The phonon dispersions of the investigated systems were calculated by the density functional perturbation theory (DFPT) method[21] via the Quantum Espresso package with PBE functional. The mobilities of carriers were calculated through the deformation potential approximation[22] with parameters that can be obtained by DFT calculations.

3 Results and discussion

3.1 Atomic structure and stability

We here investigate three configurations of the Janus $GaInX_3$ (X = S, Se, Te) as depicted in Fig. 1. As shown in Fig. 1, we can see that the Janus $GaInX_3$ is a quintuple-layer atomic material stacked in order X–Ga–X–In–X, which can be constructed by replacing the bottom In layer with the Ga layer in In_2X_3. In principle, we can also create a Janus structure with the order of X–In–X–Ga–X (from bottom to top in the vertical direction). However, our calculations show that these three Janus configurations are less stable. Therefore, in this paper, we only examine three configurations as shown in Fig. 1. The calculated structural parameters of $GaInX_3$ are listed in Table 1. The In–X and Ga–X bond lengths increase when the chalcogen atom X is moved from S to Te, which is due to the increase in the atomic size of the X atom. Besides, the Ga–X bond lengths (d_1 and d_2) are shorter the In–X bond lengths (d_3 and d_3) is also due to the difference in atomic radius between Ga and In. As a result, the lattice constant a and also the thickness Δh of $GaInX_3$ follow the same trend as they are proportional to the Ga–X and In–X bond lengths. Obtained results indicate that the lattice constant of $GaInX_3$ is from 3.74 to 4.19 Å. The lattice constant value of $GaInX_3$ is between the lattice constant value of GaX_3 and InX_3.[7]

To investigate the stabilities of the studied systems, we firstly examine the strength of chemical bonds via the analysis of their cohesive energy. In principle, $GaInX_3$ can be constructed from Ga_2X_3, which has successfully been fabricated by experiment.[6] Also, previous study suggested that Ga_2X_3 and In_2X_3 single layers are energetically favorable.[10] The cohesive energy E_c of the Janus $GaInX_3$ single-layers can be evaluated by:

$$E_c = \frac{N_{Ga}E_{Ga} + N_{In}E_{In} + N_X E_X - E_{GaInX_3}}{N_{Ga} + N_{In} + N_X}, \qquad (1)$$

where E_{GaInX_3} is the total energy of $GaInX_3$ single-layer; E_{Ga}, E_{In}, and E_X are the energies of single atoms Ga, In, and X, respectively; and N_{In}, N_{Ga}, and N_X are the atom number In, Ga, and X in the unitcell, respectively.

The obtained calculations for E_c of $GaInX_3$ single-layers are summarized in Table 1. It is found that the cohesive energy of $GaInX_3$ single-layers is quite high, from 3.49 to 4.35 eV per atom and these three structures of $GaInX_3$ are confirmed to be energetically favorable. The cohesive energy E_c decreases as the atomic size of X element increasing.
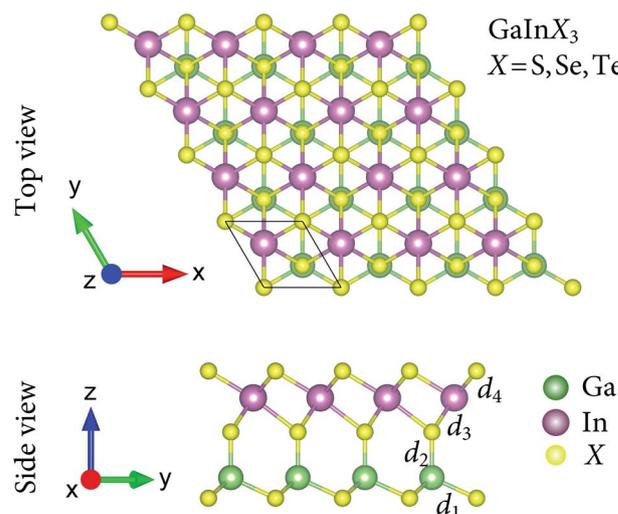

Fig. 1 Top and side views of optimized atomic structures of the Janus $GaInX_3$ (X = S, Se, Te) single-layers. The unit cell is indicated by a rhombus.

Table 1 Lattice constant a, bond length d, bond angle φ, thickness Δh, and cohesive energy of GaInS$_3$ single-layers

	a (Å)	d_1 (Å)	d_2 (Å)	d_3 (Å)	d_4 (Å)	$\varphi_{\angle \text{In–X–Ga}}$ (deg)	$\varphi_{\angle \text{X–In–X}}$ (deg)	$\varphi_{\angle \text{X–Ga–X}}$ (deg)	Δh (Å)	E_c (eV)
GaInS$_3$	3.74	2.38	2.21	2.73	2.53	127.68	95.47	103.38	6.20	4.35
GaInSe$_3$	3.90	2.52	2.34	2.84	2.66	127.53	94.40	101.92	6.60	3.95
GaInTe$_3$	4.19	2.71	2.55	3.04	2.87	127.30	93.71	101.23	7.17	3.49
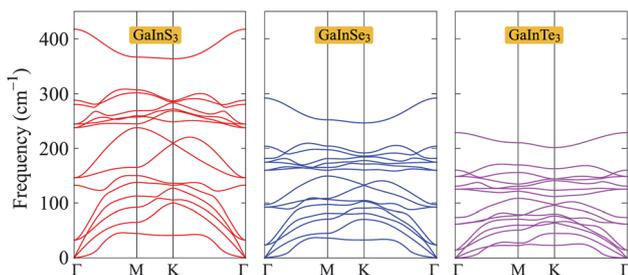
Fig. 2 Phonon dispersions of GaInS$_3$, GaInSe$_3$, and GaInTe$_3$ single-layers.

Next, we calculate the phonon spectra to evaluate the dynamical stability of GaInX$_3$ single-layers. The phonon spectra of GaInX$_3$ single-layers, which are calculated by the DFPT method,[21] are presented in Fig. 2. Note that the phonon splitting corrections[23] are not included in the present calculations. There are five atoms in the primitive cell of GaInX$_3$, therefore, its phonon dispersions contain 15 normal vibrational modes at the center of the Brillouin zone (the Γ point), including three acoustic modes in the low-frequency region and twelve optical modes in the higher frequency regions. It is known that the larger the mass atomic mass of elements, the softer the vibrations.[24] Then, vibration frequencies in the phonon dispersions of GaInX$_3$ are downshifted as the chalcogen element X changes from S to Te. As shown in Fig. 2, we can see that the phonon energies of GaInS$_3$ single-layers are lower than those of GaInSe$_3$ and GaInTe$_3$ single-layers at the same point in the Brillouin zone. More importantly, there are no negative frequencies in the phonon dispersions of all three Janus GaInX$_3$. The dynamic stabilities of materials were confirmed when the evaluated phonon dispersions contain only positive frequencies in the whole Brillouin zone. If the imaginary frequencies are available, the restoring force, which opposes the atom displacement of the atoms, will no longer exist. Obtained calculations for the phonon spectra, as depicted in Fig. 2, indicate that the Janus GaInX$_3$ single-layers are dynamically stable.

Further, we examine the elastic characteristics to elucidate the mechanical stability of the considered Janus single-layers. The elastic constants can give important information about the mechanical stability of materials. The elastic constants C_{ij} can be evaluated from the variation of energy when the small strains are applied to the equilibrium lattice state. With hexagonal structure as depicted in Fig. 1, only two independent elastic coefficients need to be estimated being C_{11} and C_{12} due to $C_{11} = C_{22}$ and $C_{66} = (C_{11} - C_{12})/2$. The small range of uniaxial strain between -0.015 and 0.015 is applied to the x and y directions (each step being 0.005). The lattice structures at each value of applied strain are optimized and obtained coefficients are so-called relaxed-ion coefficients. By polynomial fitting the small strain-dependence of energy, we can get the coefficients C_{11} and C_{12}.[25] In Table 2, we summarized the calculated results for the elastic constants C_{ij} of GaInX$_3$ single-layers. It is demonstrated that the elastic constants of GaInX$_3$ single-layers meet the Born's criteria for mechanical stability for hexagonal structures: $C_{11} > 0$ and $C_{11} - C_{12} > 0$.[26]

Young's modulus and Poisson's ratio depend greatly on the in-plane symmetric structure of the materials. The direction-dependence of Young's modulus $Y_{2D}(\varphi)$ and Poisson's ratio $\nu(\varphi)$ can be written as[27,28]

$$Y_{2D}(\theta) = \frac{C_{11}C_{22} - C_{12}^2}{C_{11}s^4 + C_{22}c^4 - s^2c^2(2C_{12} - \Delta)}, \quad (2)$$

$$\mathcal{P}(\theta) = \frac{C_{12}(s^4 + c^4) - s^2c^2(C_{11} + C_{22} - \Delta)}{C_{11}s^4 + C_{22}c^4 - s^2c^2(2C_{12} - \Delta)}, \quad (3)$$

where $\Delta = (C_{11}C_{22} - C_{12}^2)/C_{66}$, $s = \sin \varphi$, and $c = \cos \varphi$. Here, φ is the angle between the armchair and investigated directions.

The polar diagrams of $Y_{2D}(\theta)$ and $\nu(\theta)$ of GaInX$_3$ single-layers are presented in Fig. 3. We can see that the direction-dependence of $Y_{2D}(\theta)$ and $\nu(\theta)$ are perfectly circulars. This suggests that GaInX$_3$ single-layers show isotropic elastic characteristics. This is due to the 2D isotropic structures of GaInX$_2$ as shown in Fig. 1. The Janus GaInX$_3$ has a small Young's modulus, from 25.61 to 90.76 N m^{-1}. Obviously, Young's modulus of GaInX$_3$ is smaller than that of other available 2D structures, such as Janus MoSSe (113 N m^{-1})[29] or MoS$_2$ (130 N m^{-1}).[30] This indicates that the Janus GaInX$_3$ single-layers are mechanically flexible materials and their mechanical strain threshold can be large.

3.2 Electronic properties

In this section, we consider the electronic characteristics of the Janus GaInX$_3$ single-layers. Band structures of GaInX$_3$ are

Table 2 Calculated results for the elastic properties of GaInX$_3$: Elastic coefficients C_{ij}, Young's modulus Y_{2D}, and Poisson's ratio $\mathcal{P}$

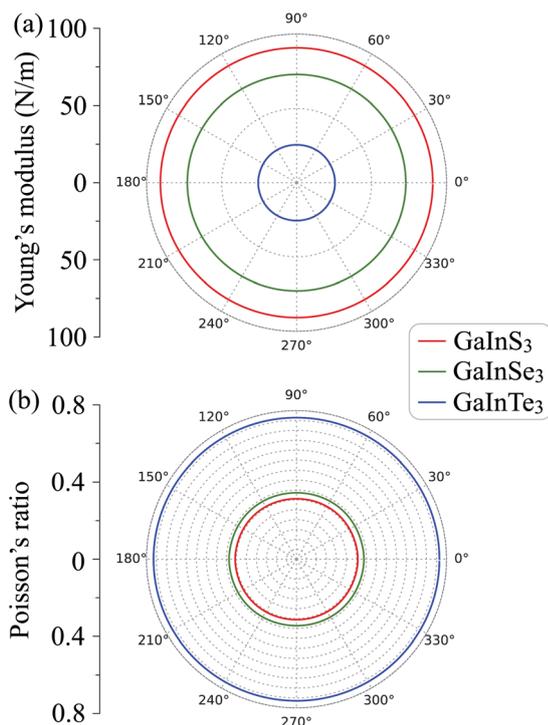|	C_{11} (N m^{-1})	C_{12} (N m^{-1})	C_{66} (N m^{-1})	Y_{2D} (N m^{-1})	$\mathcal{P}$
GaInS$_3$	100.18	30.71	34.73	90.76	0.31
GaInSe$_3$	82.15	27.69	27.23	72.82	0.34
GaInTe$_3$	52.32	37.38	7.47	25.61	0.72

Fig. 3 Direction-dependent Young's modulus (a) and Poisson's ratio (b) of GaInX$_3$ single-layers.

Table 3 The PBE and HSE06 bandgaps E_g (eV), difference in the vacuum levels $\Delta\Phi$ (eV), and work functions on the XGa-side Φ_1 (eV) and InX-side Φ_2 (eV) of GaInX$_3$ (X = S, Se, Te) single-layers

	E_g^{PBE}	E_g^{HSE06}	E_F	$\Delta\Phi$	Φ_1	Φ_2
GaInS$_3$	0.93	1.64	−2.08	1.65	4.88	6.53
GaInSe$_3$	0.47	1.20	−2.01	1.29	4.53	5.83
GaInTe$_3$	0.25	0.75	−1.18	0.90	4.16	5.06

evaluated by using the PBE and HSE06 functionals as shown in Fig. 4. Our calculations indicate that all three configurations of GaInX$_3$ are semiconductors. The electronic structures of 2D materials depend greatly on their geometry and structural parameters. At the PBE level, while GaInS$_3$ and GaInSe$_3$ single-layers exhibit the direct semiconducting characters, GaInTe$_3$ has an indirect bandgap with the conduction band minimum (CBM) lying at the Γ point and the valence band maximum (VBM) being on the ΓM-path. The PBE bandgap E_g^{PBE} of GaInX$_3$ reduces from 0.93 to 0.25 eV as the chalcogen element X changing from S to Te as listed in Table 3. The calculated band structures of GaInX$_3$ single-layers are also shown in Fig. 4. The band diagrams calculated by the PBE and HSE methods have almost the same profile. The bandgap calculated by the HSE06 functional, however, is wider than the PBE bandgap. The

bandgap calculated by the HSE06 method is considered to be more accurate than the PBE method. Our calculated results indicated that the HSE06 bandgap E_g^{PBE} of GaInX$_3$ single-layers is in the interval between 0.75 and 1.64 eV.

To get more insights into the nature of the energy bands of the considered structures, we evaluate the weighted band of GaInX$_3$ single-layers at the HSE06 level as revealed in Fig. 5. There are similarities in the weighted bands between the Janus GaInX$_3$ single-layers. It is demonstrated that the VBM of GaInX$_3$ is mainly contributed from the p-orbitals of the chalcogen atom X. Meanwhile, Ga-s orbitals have a largely contribution to the CBM of GaInX$_3$. The contribution of the orbitals of Ga and In atoms to the valence band is much smaller than that of the X-p orbitals. Also, the X-p orbitals also make a important contribution to the conduction band in the high-energy region.

One of the more important properties of electrons that we need to investigate is the work function. The work function Φ is calculated based on the formula as: $\Phi = E_{vac} - E_F$. Here, E_{vac} and E_F are the vacuum and Fermi levels, which can obtain by calculating the electrostatic potential of the material. Due to the vertical asymmetric structure, Janus single-layers possess an intrinsic built-in electric field as previously reported by Fu and co-workers.[7] Therefore, we include the dipole correction in the present calculations to treat the possible errors induced by periodic boundary condition.[31] The electrostatic potential of the Janus GaInX$_3$ single-layers with dipole correction are depicted in Fig. 6. As predicted, a distinct vacuum level difference $\Delta\Phi$ between the two sides has been found in the Janus GaInX$_3$ structures. Our calculations reveal that the $\Delta\Phi$ of GaInX$_3$ reduces when the atomic size of X element increases. As summarized in Table 3, the vacuum level difference $\Delta\Phi$ of GaInX$_3$ is from 0.90 to 1.65 eV. As a result, there is a difference between the work functions on the two different sides of
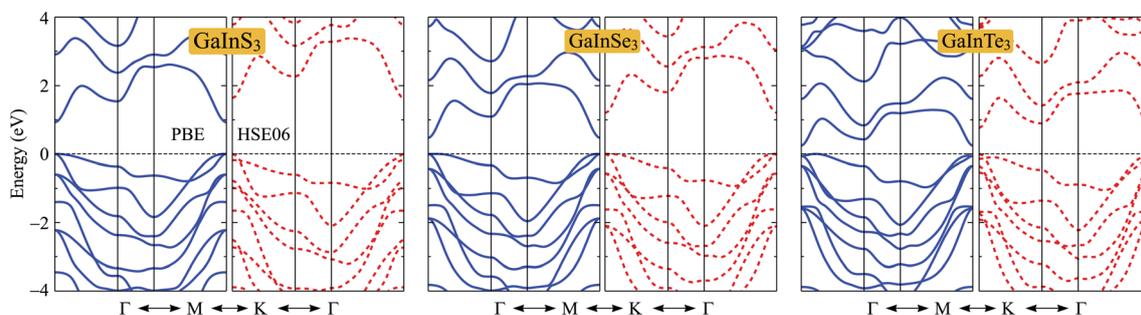

Fig. 4 Band structures along the high-symmetry direction $\Gamma - M - K - \Gamma$ of Janus GaInX$_3$ (X = S, Se, Te) single-layers at the PBE (solid lines) and HSE06 (dashed lines) levels.
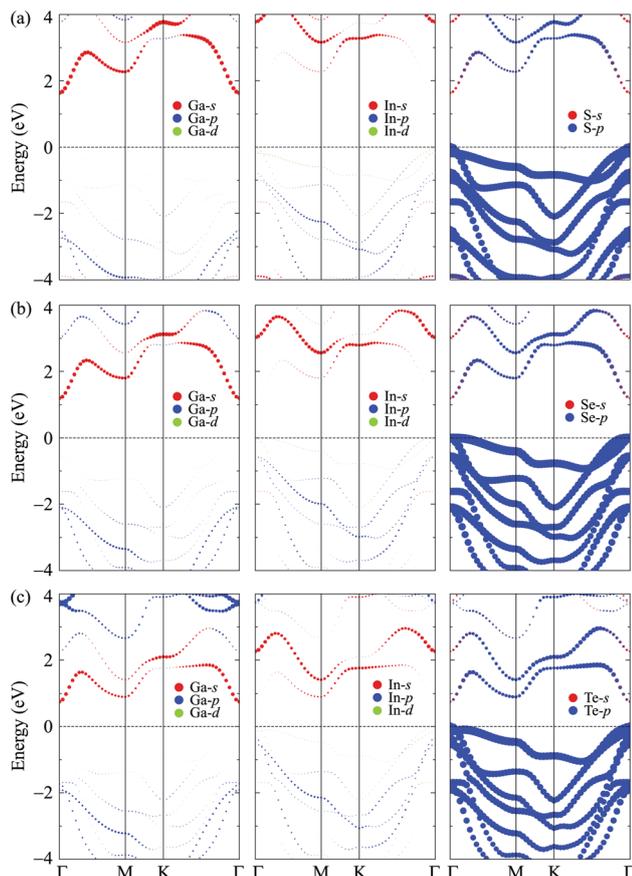
Fig. 5 Weighted bands of GaInS$_3$ (a), GaInSe$_3$ (b), and GaInTe$_3$ (c) single-layers at the HSE06 level.

GaInX$_3$. The calculated work functions on the XGa-side Φ_1 and InX-side Φ_2 of GaInX$_3$ single-layers are tabled in Table 3. We can see that, in each single-layer, Φ_1 is always smaller than Φ_2. This suggests that electrons can escape from the XGa-surface more easily than the InX-surface. Besides, the difference in the vacuum level leads to the difference in the photocatalytic performance at the two different surfaces of the Janus structures.

3.3 Transport properties

To evaluate the potential application of materials in electronic devices, we need to examine their transport properties. We here focus on the characteristics of carrier mobility, which are the most important characteristics of the transport properties. The carrier mobility of materials can be investigated by the deformation potential approximation.[22] The mobility of the carriers for the 2D materials can be expressed in the form:[32]

$$\mu_{2D} = \frac{e\hbar^3 C_{2D}}{k_B T m^* \overline{m} E_d^2},$$ (4)

where e is the elementary charge, k_B refers to the Boltzmann constant, $\hbar$ stands for the reduced Planck constant, C_{2D} is the elastic modulus, E_d is the deformation potential constant, m^* stands for the effective mass of carrier, and $\overline{m} = \sqrt{m_x m_y}$ is the
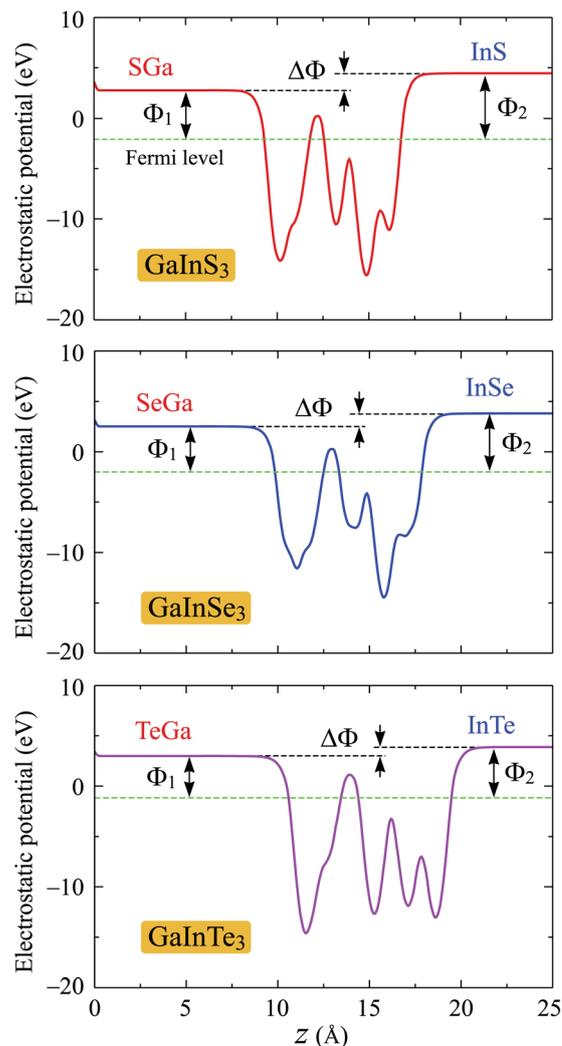

Fig. 6 Planar electrostatic potential of the Janus GaInX$_3$ (X = S, Se, Te) single-layers with dipole correction. $\Delta\Phi$ is the difference in the vacuum levels between the XGa and InX sides.

average effective mass. The calculations for the carrier mobility were performed at room temperature ($T = 300$ K). The transport characteristics were investigated along the two transport directions.

To calculate the carrier mobility μ_{2D} as expressed in eqn (4), we first evaluate the effective mass of carriers, which strongly affects the mobilities of carriers. The effective masses of carriers can be attained by fitting parabolic function to the CBM (electron) and VBM (hole) via the formula as follows:

$$\frac{1}{m^*} = \frac{1}{\hbar^2} \left| \frac{\partial^2 E(k)}{\partial k^2} \right|,$$ (5)

where $E(k)$ is the wave-vector k-dependence of energy at the CBM/VBM (in the $k_x k_y$ plane). The effective mass depends strongly on the energy bands around the band-edges. The effective masses of carriers are heavy if the energy bands near the band-edges are flat. This is due to small the second derivative $\partial^2 E(k)/\partial k^2$.

Table 4 Effective mass m^* of electron and hole (m_0), elastic modulus C_{2D} (N m^{-1}), deformation potential constant E_d (eV), and carrier mobility μ (cm^2 V^{-1} s^{-1}) along the x/y-direction of GaInX$_3$ (X = S, Se, Te) single-layers. m_0 is the free electron mass

		m_x^*	m_y^*	C_{2D}^x	C_{2D}^y	E_d^x	E_d^y	μ_x	μ_y
GaInS$_3$	Electron	0.29	0.29	66.57	66.58	−9.12	−9.12	202.87	203.08
	Hole	2.69	2.69	66.57	66.58	−7.51	−7.59	3.20	3.13
GaInSe$_3$	Electron	0.18	0.18	54.84	54.86	−8.01	−8.01	580.82	580.55
	Hole	0.47	0.47	54.84	54.86	−7.33	−7.42	22.88	22.33
GaInTe$_3$	Electron	0.15	0.15	43.38	43.43	−8.70	−8.69	530.03	532.18
	Hole	0.23	0.23	43.38	43.43	−7.82	−7.98	117.52	113.06

The effective masses of carriers of GaInX$_3$ single-layers are summarized in Table 4. It is found that the effective mass of both electron and hole is highly directional isotropic. This is due to the in-plane isotropic lattice of the Janus GaInX$_3$ single-layers. However, the effective mass of the electron is much smaller than that of hole, particularly in the case of GaInS$_3$ single-layer. The smaller the carrier mass, the faster carriers respond to the external field, and as a result, they have high mobility. As listed in Table 4, we can see that GaInTe$_3$ has the smallest electron effective mas, 0.15 m_0. The electron effective mass of GaInS$_3$ and GaInTe$_3$ is found to be 0.29 m_0 and 0.18 m_0, respectively.

Along with the effective mass, the carrier mobility depends also on the elastic modulus C_{2D} and deformation potential constant E_d as presented in eqn (4). The elastic modulus C_{2D} is given by

$$C_{2D} = \frac{1}{V}\frac{\partial^2 E}{\partial \varepsilon_{uni}^2}, \qquad (6)$$

where E is the total energy, V is the area of simulated unitcell, and ε_{uni} is the small uniaxial strain along the transport direction x/y. In our calculations, ε_{uni} from −1% to 1% is applied to the transport directions.

The deformation potential constant E_d is written in the form:

$$E_d = \frac{\Delta E_{edge}}{\varepsilon_{uni}}, \qquad (7)$$

where ΔE_{edge} indicates the changing of the band edge energy referencing to the vacuum level. The values of the C_{2D} and E_d are obtained by fitting the strain-dependent energy and band-edge position.[32,33]

The strain-dependent energy change and band edge positions of all three Janus structures GaInX$_3$ are shown in Fig. 7. It is found that there is no significant difference in elastic modulus along the x and y directions in each single-layer. The deformation potential constant of GaInX$_3$ is also high directional isotropic. This is also due to the in-plane isotropic lattice of the investigated systems. However, there is a small difference in the E_d of electron and hole in all three investigated structures. The calculated results for the C_{2D} and E_d are summarized in Table 4.

In Table 4, we list the calculated results for the carrier mobility of GaInX$_3$ single-layers along the two transport directions. It is found that the mobility of both electron and hole of GaInX$_3$ is highly directional isotropic. There is no significant difference between carrier mobilities along the x and y directions. Due to the largely difference in the effective mass and also deformation potential constant between electron and hole, it is calculated that the electron mobility is much higher than that the hole mobility. The electron mobility of GaInSe$_3$ is calculated to be up to about 580 cm^2 V^{-1} s^{-1} and all Janus GaInX$_3$ structures possess electron mobility in excess of 200 cm^2 V^{-1} s^{-1}. It is also worth noting that, with electron mobility of about 200 cm^2 V^{-1} s^{-1}, MoS$_2$ was able to
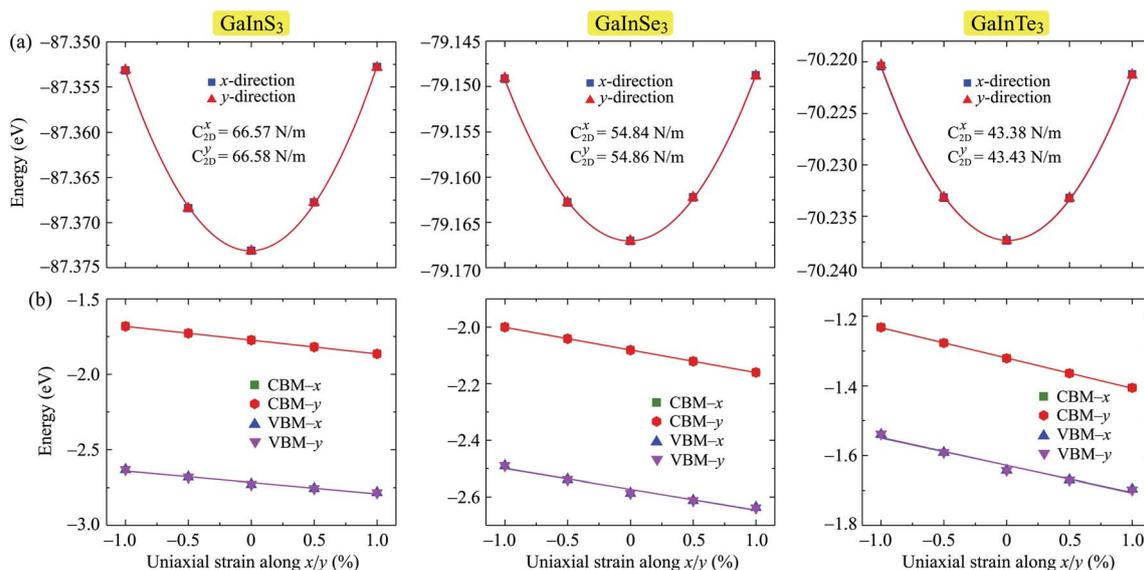
Fig. 7 Strain-dependent total energy (a) and band-edge positions (b) of GaInX$_3$ single-layers along two transport directions x and y.

perfectly apply to high-performance electronic devices as previously reported by Radisavljevic and co-workers.[34] This suggests that the Janus $GaInX_3$ single-layer could be potential materials for applications in nanoelectronic devices.

4 Conclusion

In this paper, we systematically considered the structural, electronic, and transport properties of the novel Janus $GaInX_3$ single-layers using the DFT calculations. The obtained results indicated that the structure of Janus $GaInX_3$ single-layers was confirmed to be stable and their elastic properties are highly directional isotropic. At the equilibrium states, $GaIn_3$ single-layers are semiconductors with a small bandgap. Due to the asymmetric structure, there exists a distinct vacuum level difference on the two sides of the Janus $GaInX_3$. Carrier mobility of $GaInX_3$ is also highly isotropic along the two transport directions and their electron mobility can be up to about 580 cm^2 V^{-1} s^{-1}, which is suitable for applications in nanoelectronics.

Conflicts of interest

There are no conflicts to declare.

Acknowledgements

References

1 N. A. Poklonski, S. A. Vyrko, A. I. Siahlo, O. N. Poklonskaya, S. V. Ratkevich, N. N. Hieu and A. A. Kocherzhenko, *Mater. Res. Express*, 2019, **6**, 042002.

2 T. V. Vu, C. V. Nguyen, H. V. Phuc, A. A. Lavrentyev, O. Y. Khyzhun, N. V. Hieu, M. M. Obeid, D. P. Rai, H. D. Tong and N. N. Hieu, *Phys. Rev. B*, 2021, **103**, 085422.

3 T. V. Vu, V. T. T. Vi, H. V. Phuc, A. I. Kartamyshev and N. N. Hieu, *Phys. Rev. B*, 2021, **104**, 115410.

4 T. N. Bich, S. S. Kubakaddi, L. Dinh, N. N. Hieu and H. V. Phuc, *Phys. Rev. B*, 2021, **103**, 235417.

5 A.-Y. Lu, H. Zhu, J. Xiao, C.-P. Chuu, Y. Han, M.-H. Chiu, C.-C. Cheng, C.-W. Yang, K.-H. Wei, Y. Yang, Y. Wang, D. Sokaras, D. Nordlund, P. Yang, D. A. Muller, M.-Y. Chou, X. Zhang and L.-J. Li, *Nat. Nanotechnol.*, 2017, **12**, 744.

6 G. Almeida, S. Dogan, G. Bertoni, C. Giannini, R. Gaspari, S. Perissinotto, R. Krahne, S. Ghosh and L. Manna, *J. Am. Chem. Soc.*, 2017, **139**, 3005–3011.

7 C.-F. Fu, J. Sun, Q. Luo, X. Li, W. Hu and J. Yang, *Nano Lett.*, 2018, **18**, 6312–6317.

8 P. Zhao, Y. Ma, X. Lv, M. Li, B. Huang and Y. Dai, *Nano Energy*, 2018, **51**, 533–538.

9 J. Xiao, H. Zhu, Y. Wang, W. Feng, Y. Hu, A. Dasgupta, Y. Han, Y. Wang, D. A. Muller, L. W. Martin, P. Hu and X. Zhang, *Phys. Rev. Lett.*, 2018, **120**, 227601.

10 L. Hu and X. Huang, *RSC Adv.*, 2017, **7**, 55034–55043.

11 G. Liu, Z. Zhang, H. Wang, G.-L. Li, J.-S. Wang and Z. Gao, *J. Appl. Phys.*, 2021, **130**, 105106.

12 J. Zhao, X. Huang, Y. Yin, Y. Liao, H. Mo, Q. Qian, Y. Guo, X. Chen, Z. Zhang and M. Hua, *J. Phys. Chem. Lett.*, 2021, **12**, 5813–5820.

13 W. Ding, J. Zhu, Z. Wang, Y. Gao, D. Xiao, Y. Gu, Z. Zhang and W. Zhu, *Nat. Commun.*, 2017, **8**, 14956.

14 P. Wang, H. Liu, Y. Zong, H. Wen, J.-B. Xia and H.-B. Wu, *ACS Appl. Mater. Interfaces*, 2021, **13**, 34178–34187.

15 T. V. Vu and N. N. Hieu, *J. Phys.: Condens. Matter*, 2022, **34**, 115601.

16 P. Giannozzi, S. Baroni, N. Bonini, M. Calandra, R. Car, C. Cavazzoni, D. Ceresoli, G. L. Chiarotti, M. Cococcioni, I. Dabo, A. D. Corso, S. de Gironcoli, S. Fabris, G. Fratesi, R. Gebauer, U. Gerstmann, C. Gougoussis, A. Kokalj, M. Lazzeri, L. Martin-Samos, N. Marzari, F. Mauri, R. Mazzarello, S. Paolini, A. Pasquarello, L. Paulatto, C. Sbraccia, S. Scandolo, G. Sclauzero, A. P. Seitsonen, A. Smogunov, P. Umari and R. M. Wentzcovitch, *J. Phys.: Condens. Matter*, 2009, **21**, 395502.

17 P. E. Blöchl, *Phys. Rev. B: Condens. Matter Mater. Phys.*, 1994, **50**, 17953.

18 J. P. Perdew, K. Burke and M. Ernzerhof, *Phys. Rev. Lett.*, 1996, **77**, 3865.

19 J. Heyd, G. E. Scuseria and M. Ernzerhof, *J. Chem. Phys.*, 2003, **118**, 8207.

20 S. Grimme, *J. Comput. Chem.*, 2006, **27**, 1787.

21 T. Sohier, M. Calandra and F. Mauri, *Phys. Rev. B*, 2017, **96**, 075448.

22 J. Bardeen and W. Shockley, *Phys. Rev.*, 1950, **80**, 72.

23 T. Sohier, M. Gibertini, M. Calandra, F. Mauri and N. Marzari, *Nano Lett.*, 2017, **17**, 3758–3763.

24 A. Molina-Sánchez and L. Wirtz, *Phys. Rev. B: Condens. Matter Mater. Phys.*, 2011, **84**, 155413.

25 K.-A. N. Duerloo, M. T. Ong and E. J. Reed, *J. Phys. Chem. Lett.*, 2012, **3**, 2871–2876.

26 R. C. Andrew, R. E. Mapasha, A. M. Ukpong and N. Chetty, *Phys. Rev. B: Condens. Matter Mater. Phys.*, 2012, **85**, 125428.

27 N. T. Hung, A. R. T. Nugraha and R. Saito, *J. Phys. D: Appl. Phys.*, 2018, **51**, 075306.

28 P. Xiang, S. Sharma, Z. M. Wang, J. Wu and U. Schwingenschlögl, *ACS Appl. Mater. Interfaces*, 2020, **12**, 30731.

29 S.-D. Guo, *Phys. Chem. Chem. Phys.*, 2018, **20**, 7236–7242.

30 R. C. Cooper, C. Lee, C. A. Marianetti, X. Wei, J. Hone and J. W. Kysar, *Phys. Rev. B: Condens. Matter Mater. Phys.*, 2013, **87**, 035423.

31 L. Bengtsson, *Phys. Rev. B: Condens. Matter Mater. Phys.*, 1999, **59**, 12301.

32 W. Wan, S. Zhao, Y. Ge and Y. Liu, *J. Phys.: Conden. Matter*, 2019, **31**, 435501.

33 S.-D. Guo, W.-Q. Mu, Y.-T. Zhu, R.-Y. Han and W.-C. Ren, *J. Mater. Chem. C*, 2021, **9**, 2464–2473.

34 B. Radisavljevic, A. Radenovic, J. Brivio, V. Giacometti and A. Kis, *Nat. Nanotechnol.*, 2011, **6**, 147–150.